Article

J. Mex. Chem. Soc. **2021**, *65*(1)
Special Issue

ISSN-e 2594-0317

Synthesis and Characterization of ZnAPO-34 and SAPO-34: Effect of Zn on the Acidity and Catalytic Activity in the MTO Reaction

Misael García Ruiz*[1], Julia Aguilar Pliego*[2], Carlos Márquez Álvarez[3], Marisol Grande Casas[3], Enrique Sastre de Andrés[3]

[1]Doctorado en Ciencia de Materiales de la Facultad de Química, Universidad Autónoma del Estado de México, Paseo Colón Esquina Paseo Tollocan S/N, Toluca Estado de México, México, C.P. 50000.
[2]Área de Química Aplicada, Departamento de Ciencias Básicas, UAM-A, San Pablo 180, C.P. 02200, Cd de México.
[3]Instituto de Catálisis y Petroleoquímica, CSIC, C/Marie Curie 2, 28049 Madrid, España.

***Corresponding author:** Misael García Ruiz, email: misa_gr@hotmail.com; Julia Aguilar Pliego, email: apj@azc.uam.mx

Received July 11th, 2020; Accepted November 6th, 2020.

DOI: http://dx.doi.org/10.29356/jmcs.v65i1.1261

Abstract. SAPO-34 and ZnAPO-34 materials (Zn incorporated by isomorphic substitution in AlPO-34 material) were synthesized by hydrothermal synthesis using triethylamine (TEA) as the structure directing agent (SDA). The structure presented by both materials is isomorphic to the chabazite zeolite (CHA). However, they have different properties such as textural properties (Z34 and S34 presented a surface area of 485 and 603 m^2/g, respectively), different crystal sizes and acid properties. The physicochemical properties of the zeotypes were studied using XRD (X-ray diffraction), N_2 adsorption-desorption, temperature programmed desorption of NH_3 and SEM (Scanning Electron Microscopy). The catalytic performance of these catalysts was studied in the MTO reaction at 400 °C and atmospheric pressure using a WHSV of 2.12 h^{-1} in a fixed bed reactor. The incorporation of Zn had an important effect on acidity, generating a higher density of acid sites, increasing selectivity to light olefins. It was observed that when the crystal size decreases (ZnAPO-34), 100 % mol methanol conversion is obtained at short reaction times. The ZnAPO-34 material had a smaller crystal size (0.5 µm) and selectivity for olefins of 78 mol %. On the other hand, the SAPO-34 catalyst showed a larger crystal size (1.5 µm) and lower selectivity to olefins (72 mol %). The Z34 catalyst was compared with a previously reported MeAPSO-36 material, the latter was selective for the formation of aromatic compounds and lower selectivity to olefins (35 % mol) due to the presence of larger channels and lower density of acid sites.
Keywords: Methanol conversion; zeotypes; light olefins; CHA structure; SAPO-34; MeAPO-34.

Resumen. En este trabajo se han sintetizado materiales SAPO-34 y ZnAPO-34 (Zn incorporado por sustitución isomórfica en material AlPO-34), mediante síntesis hidrotérmica usando trietilamina (TEA) como agente director de la estructura. La estructura presentada por ambos materiales es isomorfa a la de una zeolita chabazita. Sin embargo, ambos materiales tienen diferentes propiedades texturales (Z34 y S34 presentaron un área superficial de 485 y 603 m^2/g, respectivamente), diferentes tamaños de cristal y distinta acidez. Las propiedades fisicoquímicas de los catalizadores se estudiaron mediante DRX (difracción de Rayos X), adsorción-desorción de N_2, desorción programada a temperatura de NH_3 y SEM (Microscopia electrónica de barrido). El rendimiento catalítico de los catalizadores se estudió en la reacción de transformación de metanol a olefinas (MTO) a 400 °C y presión atmosférica en un reactor de lecho fijo operando con un WHSV de 2.12 h^{-1}. La incorporación de Zn tuvo un efecto importante en la acidez generando una mayor densidad de sitios ácidos y aumentando la

J. Mex. Chem. Soc. **2021**, *65*(1)
Special Issue

ISSN-e 2594-0317

selectividad a olefinas ligeras. Se observó que cuando el tamaño del cristal disminuye (ZnAPO-34), se obtiene una conversión de metanol del 100 % mol a tiempos cortos de reacción. El material ZnAPO-34 presentó un tamaño de cristal más pequeño (0.5 µm) y selectividad para olefinas de 78 % mol. Por otro lado, el catalizador SAPO-34 mostró un tamaño de cristal más grande (1.5 µm) y menos selectividad a olefinas (72 % mol). El catalizador Z34 fue comparado con un material MeAPSO-36 reportado anteriormente, que presentaba alta selectividad hacia la formación de compuestos aromáticos y menor selectividad a olefinas (35 % mol), debido a la presencia de canales de mayor tamaño y menor densidad de sitios ácidos.
Palabras clave: Conversión de metanol; zeotipos; olefinas ligeras; estructura CHA; SAPO-34; MeAPO-34.

List of Abbreviations

MTO= methanol to olefins.
$AlPO_4$-n= microporous crystalline aluminophosphate.
MeAPO= microporous crystalline aluminophosphate containing a transition metal ion, MeAPSO.
MeAPSO= microporous crystalline aluminophosphate doubly substituted by two transition metal iones
WHSV= weight hourly space velocity.
SEM = scanning electron microscopy.
ICP-OES= inductively coupled plasma optical emission spectrometry.
BET= Brunauer – Emmett – Teller equation.
SM= substitution isomorphic.
XRD= X-ray diffraction.
TPD= temperature programmed desorption.
TGA= thermogravimetric analyses.
DTG= derivate thermogravimetric.
SDA= structure-directing agent.
MR= Member rings.

Introduction

Light olefins such as ethylene and propylene are raw materials in the petrochemical industry which have considerable importance in the production of polymeric materials [1-4]. Limitation for crude oil sources and the prediction of growth in oil prices in the future are the reasons for the raised attention to the development of new technologies for the production of light olefins from non-oil sources [5]. Methanol-to-olefins (MTO) technology is an alternative process to effectively alleviate current petroleum supply–demand issues due to the conventional preparation of lower olefins that uses petroleum cracking [6,7]. Because of the hydrothermal stability, acidity, and molecular selectivity of zeolites and zeotype molecular sieves, they have been widely used in industrial processes such as the catalyst of MTO process. In addition to the acidity, the crystal size of zeotype is also an important factor that may influence the catalytic performance, especially the catalyst lifetime in the MTO, reaction due to coke formation. Modified zeotypes with small crystal size have been reported to exhibit a prolonged lifetime in MTO conversion due to their good resistance to deactivation by coke.[8]

Aluminophosphate (AlPO) microporous molecular sieves have been reported for the first time in 1982 [9]. Since the frameworks of AlPO molecular sieves are neutral, they usually have no catalytic capabilities. Silicon substitution into AlPO framework results in the formation of silicoaluminophosphate (SAPO) molecular sieves. The substitution of P^{5+} with Si^{4+} produces Brönsted acid sites and therefore, leads to catalytic capability. [10,11]

Because of hydrothermal stability, acidity, and molecular selectivity of SAPO molecular sieves, they have been widely used in industrial processes such as the catalyst of MTO process. Especially, SAPO-34, a microporous silicoaluminophosphate zeotype material with large cavities (9.4 Å in diameter) connected by small 8-ring pore openings (3.8 x 3.8 Å), which shows high selectivity for the lower olefins, because of its small pore entrances [12]. It is the best catalyst for MTO process due to the small pore size, moderate acidity and well thermal/hydrothermal stability [13]. However, despite the high selectivity, the narrow pore opening limits the

J. Mex. Chem. Soc. **2021**, *65*(1)
Special Issue

ISSN-e 2594-0317

mass transport in the SAPO-34 crystal and causes large hydrocarbon molecules and coke traps within the cages and thereby lead to rapid deactivation [14].

In general, the catalyst acidity, pore size and shape, particle size, and presence of heteroatoms (Ni, Co, Mn, Fe, etc.) are among the many factors that play major roles in determining activity and selectivity [15]. Until now, a multitude of metals ion including Zn, Ca, Cu, La, Au, Ti, Cr, Fe, Mg, Ni, Mn, Ce, Zn, W, Mn, Zr, Co, Ba, and Sr have been used as a promoter for modification of SAPO-34 catalytic properties incorporated by isomorphic substitution [3,16-19]. Isomorphic substitution of framework Al^{3+} and P^{5+} ions by metal cations or silicon, respectively, produce the MeAPSO material. Since Zn is an active metal to promote the aromatization of methanol, the physical mixtures of SAPO-34 and ZnO were used for MTO reaction to increasing the ratio of ethene to propene, to gain a deep understanding of the synergetic effect of various catalyst functions [20]. Metal heteroatom modification, through isomorphous substitution (MeAPSO-34) or ion exchange and impregnation (Me/SAPO-34), has been extensively investigated to tune the acidity and local structure of SAPO-34 cavity improving the reaction product and enhance the catalyst lifetime [21]. Xu et al., [22] demonstrated that incorporation Zn ions had great effects on crystal size and acidity of the molecular sieves. The higher selectivity is attributed to framework distortion and acidity modification after the incorporation of zinc. In this sense, the incorporation of Zn^{2+} ions showed a promising modification effect for the MTO catalysts.

Generally, the synthesis of SAPO-34 is performed in the presence of organic templates [23], tetraethylammonium hydroxide (TEAOH), dipropylamine (DPA), diethylamine DEA and tripropylamine (TEA). Several previous reports [18,20] show that using TEA as the structure directing agent (SDA) forms smaller SAPO-34 crystals (200 nm). MTO process is strongly influenced by the crystal size providing catalytic performance and olefins selectivity. [6,24]

In the present study, we report on the synthesis of SAPO-34 catalysts and the incorporation of Zn ions in the AlPO-34 framework by isomorphic substitution (ZnAPO-34) using TEA as SDA. Both catalysts were evaluated in the MTO reaction and the presence of Zn was related to acidity and its influence on selectivity to olefins.

Experimental

Materials

The reagents used for the preparation of zeolites are tetraethyl orthosilicate (TEOS, 98 %, Aldrich), aluminum hydroxide hydrated ($Al(OH)_3$, Sigma-Aldrich), zinc acetate dihydrate ($Zn(CH_3COO)_2$ $2H_2O$, 99 % Sigma Aldrich), triethylamine (TEA, 99 %, Aldrich), Phosphoric acid (H_3PO_4, 85 wt. % in H_2O, Aldrich).

Synthesis of SAPO-34

SAPO-34 material was synthesized according to the reported procedure [22]. The gels were prepared using phosphoric acid (H_3PO_4, 85 % in water, Aldrich), Hydrated aluminum hydroxide ($Al(OH)_3$-xH_2O, Aldrich) and triethylamine (TEA, 99 %, Aldrich) with a molar composition of 1.0 P: 1.0 Al: 0.2 Si: 0.8 TEA :10 H_2O.

In a typical synthesis H_3PO_4 and $Al(OH)_3$-xH_2O were dissolved in deionized H_2O under continuous stirring for 15 min. Upon dissolution, TEOS was slowly added to the solution under vigorous stirring until a homogeneous gel was achieved. Finally, the SDA was added to the gel dropwise and then rapidly with vigorous stirring by 1 h. Gels were then placed in Teflon (PTFE) lined stainless steel autoclaves and heated for 18 h at 160 °C. Then products were filtered, washed with distilled water, and dried at 100 °C for one night. As-prepared samples were calcined at 550 °C for 6 h under an air flow. Previously, the sample has been heating with a rate of 1 °C/min under a N_2 flow and maintained for 1 h at 550 °C under this atmosphere. This sample was denoted as S34.

Synthesis of MeAPSO-34 material

MeAPSO-34 sample was synthesized by hydrothermal treatment similarly to S34 sample however, the gel molar composition was 1.0 P: 0.1 Zn: 0.9 Al: 0.2 Si: 0.8 TEA: 10 H_2O. In a typical synthesis H_3PO_4 and

J. Mex. Chem. Soc. **2021**, *65*(1)
Special Issue

ISSN-e 2594-0317

$Al(OH)_3$-xH_2O were dissolved in deionized H_2O under continuous stirring for 15 min. Upon dissolution, zinc diacetate ($Zn(CH_3$-$COO)_2$-$2H_2O$) was slowly added until a homogeneous gel and TEOS were added under continuous stirring for 15 min more. Finally, the SDA was added to the gel dropwise and then rapidly with vigorous stirring by 1 h. Gels were then placed in Teflon (PTFE) lined stainless steel autoclaves and heated for 18 h at 160 °C. Finally, the samples were calcined under the same conditions mentioned previously. This catalyst was denoted as Z34.

Catalyst characterization

Powder X-ray diffraction (PXRD) patterns were collected with an XPert Pro PANalytical diffractometer (CuKα1 radiation = 0.15406 nm). Scanning electron microscopy (SEM) images were recorded on a Hitachi S-3000N microscope. A transmission electron microscopy (TEM) study was carried on a JEOL 2100F microscope operating at 200 KV. Nitrogen adsorption/desorption isotherms were measured at 77 K in a Micromeritics ASAP 2020 device. Before the measurement, the previously calcined sample was degassed at 350 °C under a high vacuum for at least 10 h. Surface areas were estimated by the BET method whereas microporous and external surface areas were estimated by applying the t-plot method.

The Al, Si, P and Zn concentrations of samples were obtained by inductively coupled plasma-optical emission spectroscopy (ICP-OES) with an Optima 3300 DV Perkin Elmer. Temperature programmed desorption of ammonia (NH_3-TPD) was conducted using a Micrometrics Autochem II chemisorption analysis equipment. Typically, 100 mg of sample pellets (30–40 mesh) were pretreated at 550 °C for 1 h in helium flow (25 mL/min) and then cooled to the adsorption temperature (177 °C). A gas mixture of 5.0 vol.% NH_3 in He was then allowed to flow over the sample for 4 h at a rate of 15 mL/min. Afterward, the sample was flushed with a 25 ml/min helium flow for 30 min while maintaining the temperature at 177 °C to remove weakly adsorbed NH_3, and finally the temperature was increased to 550 °C at a rate of 10 °C/min. Thermogravimetric analysis (TGA) was carried out at heating of 30 °C to 900 °C with a rate of 20 °C/min under air flow and registered in a PerkinElmer TGA7 instrument.

MTO catalytic testing conditions

Zeotype materials were tested as catalysts in the conversion of methanol at 400 °C in a Microactivity reaction device (PID Eng & Tech) consisting of a fixed bed reactor completely automated and controlled from a computer. The reactor outlet is connected to a gas chromatograph to analyze the reaction products. N_2 was used as a stripping gas under a controlled flow. The methanol was fed as a liquid using an HPLC pump (Gilson 307). The methanol was converted to the gas phase and mixed with the N_2 stream in a preheater at 180 °C to generate a gas mixture with a constant molar ratio of methanol/N_2 of 4. Before the reaction, the catalysts were activated at 550 ° C for 1 h low air flow to remove any trace of organic molecules or moisture adsorbed within the pores of the catalyst. The weight of the catalyst (sieved in a 20-30 mesh, corresponding to a particle size between 0.84 and 0.59 mm) and the flow of methanol was optimized to achieve a space velocity (WHSV) of 2.12 h^{-1}.

The reaction products were analyzed online by gas chromatography with a VARIAN CP3800 chromatograph. The device is equipped with two columns: (i) a Petrocol DH50.2 capillary column connected to an FID detector, and (ii) a HayesepQ packed column (2 m length, 3.17 mm (1/8 ") diameter external and 2 mm internal diameter) connected to a TCD detector, to analyze hydrocarbons and oxygenated products, respectively.

Results and discussion

X-ray diffraction

The X-ray powder diffraction patterns of the as-synthesized samples (Fig. 1) confirmed the structure type SAPO-34 (CHA structure) in both materials (S34 and Z34). The patterns and peak positions match the patterns were compared with the theoretical database of the International Zeolite Association (IZA). By adding Zn, it seems that the contribution of Zn heteroatoms in completing the structure is important, as the presence of

J. Mex. Chem. Soc. **2021**, *65*(1)
Special Issue

ISSN-e 2594-0317

Zn oxide is not observed in diffraction patterns. And if the Zn were out of the structure the crystallinity would be diminished [25]. Benvindo et al., [26] synthesized SAPO-34 and MeAPSO-34, they demonstrate that the processes of incorporating Zn into the SAPO-34 structure did not cause structural changes. This may be due to the low built-in metal content that was insufficient to promote global distortion in the network, as in our case where the amount of Zn is small.

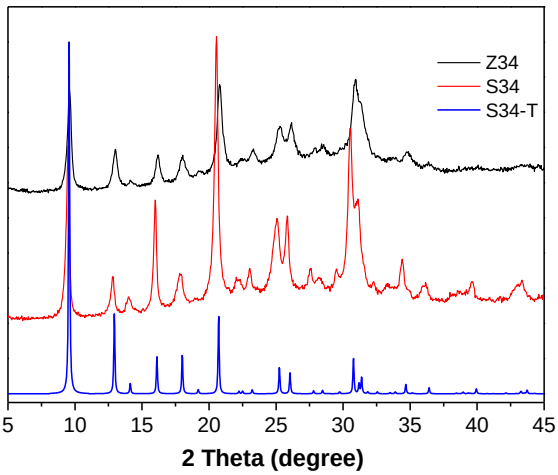

Fig. 1. XRD patterns of Z34, S34 and S34-T (IZA reference of SAPO-34 [*http://www.iza-structure.org/*]).

N_2 adsorption-desorption

Both samples were studied by N_2 adsorption/desorption isotherms at 77 K order to determine their textural properties. Isotherms of S34 and Z34 samples are plotted in Fig. 2. Samples present type I isotherms (according to the IUPAC classification [27]), corresponding to microporous materials. At higher relative pressures, the N_2 adsorption-desorption curve of samples exhibits hysteresis H4-type, which is characteristic of molecular sieves with the formation of inter or intracrystalline mesopores [28,29]. The adsorption–desorption isotherm for samples shows a strong enhancement in adsorption with hysteresis at high relative pressures due to the intercrystalline porosity typical of nanocrystalline materials.

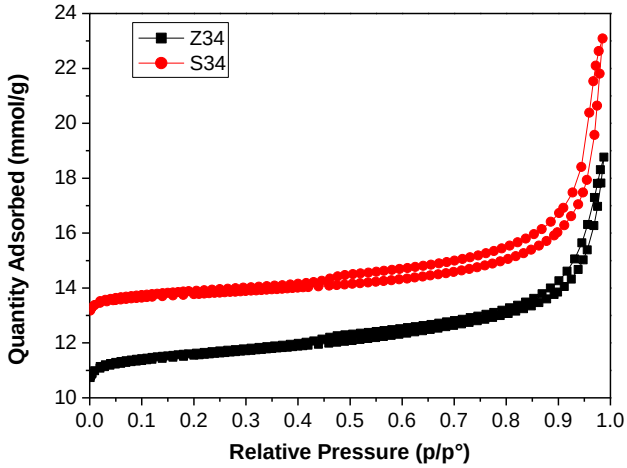

Fig. 2. N_2 adsorption–desorption isotherms of Z34 and S34 materials.

J. Mex. Chem. Soc. **2021**, *65*(1)
Special Issue

ISSN-e 2594-0317

The micropore volumes and BET areas for the samples prepared are summarized in Table 1. As it is shown, the Z34 sample obtained from Zn incorporation exhibits a BET surface area of 485.2 m^2/g, which is smaller than those typical of S34 material (603.5 m^2/g). This would be due to larger Zn ion incorporation into the SAPO-34 framework in place of smaller Al and Si ions which can reduce the surface area [30]. The sample with larger crystallites (Z34) possesses a lower surface area and all the samples show lower non-microporous (external) surface, values characteristic of this type of materials.

Table1. Chemical composition (ICP-OES) and textural properties (N_2 adsorption-desorption) of the prepared samples.

Catalyst	% wt.				(Si + P)/Al ratio	S_{BET} (m^2*g^{-1})	S_{micro} ($m^2 \cdot g^{-1}$)[a]	S_{ext} ($m^2 \cdot g^{-1}$)[a]
	% Al	% P	% Zn	% Si				
S34	18.2	23.7	-	2.1	1.24	603.5	564.4	39.1
Z34	21.6	21.2	2.5	2.4	0.95	485.2	414.5	70.7

Scanning electron microscopy (SEM)

The morphology of the different samples has been determined by SEM (Fig. 3). The crystal sizes obtained were influenced by Zn and Si content (MeAPSO). As it can be observed in this figure, all the samples had uniform cubic crystals with chabazite-like structures. S34 sample presented an average crystal size of 1.6 µm. However, the crystallite size decreased in Z34 sample. Thus, the introduction of Zn species reduces the crystal size of SAPO-34, indicating that the presence of Zn species in the initial gel may increase the nucleation rate [19]. These observations are in good agreement with XRD data previously presented, confirming the smaller crystal size of sample Z34. Both analyses indicate that the prepared samples possess similar structures at microscopic and macroscopic levels.

On the other hand, SEM images of Z34 material presented a reduction in size and surface smoothness (roughness, kink and steps) of crystallites. According to the SEM images presented in Fig. 3**a)**, sample S34 presented the largest crystals [31]. Since diffusion is an important process in the MTO reaction, such a distinct difference in the particle size could be an important factor in the MTO reaction [32].

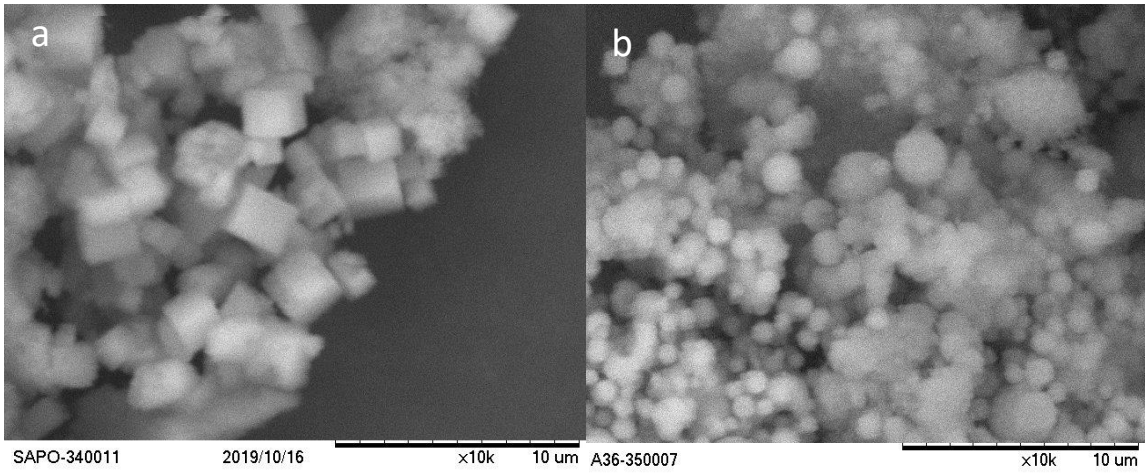

Fig. 3. SEM images of samples S34 **a)** and Z34 **b)**.

J. Mex. Chem. Soc. **2021**, *65*(1)
Special Issue

ISSN-e 2594-0317

TGA and DTG analysis

Thermogravimetric analyses (TGA) were performed aiming to verify the incorporation of the SDA molecules in the structure of the as-made samples and their subsequent complete elimination after and before calcination. The TGA and DTG curves of both materials not calcined are shown in Figures 4**a)** and 4**b)**, respectively. TGA profiles are strongly influenced by the Zn incorporation. In both figures, three weight losses are observed. The first weight loss, at temperatures below 150 °C (step I), can be attributed the desorption of adsorbed water. The second weight loss, between 400 and 550 °C (step II) is due to the decomposition of the template in each case (TEA) and, finally, the third weight loss at temperatures higher than 600 °C (step III) has been associated with the further removal of organic residues occluded in the channels and cages of the materials caused by combustion [33]. Template removal is associated with OH generation, so the template degradation temperature may predict the Brönsted acidity strength. [34]

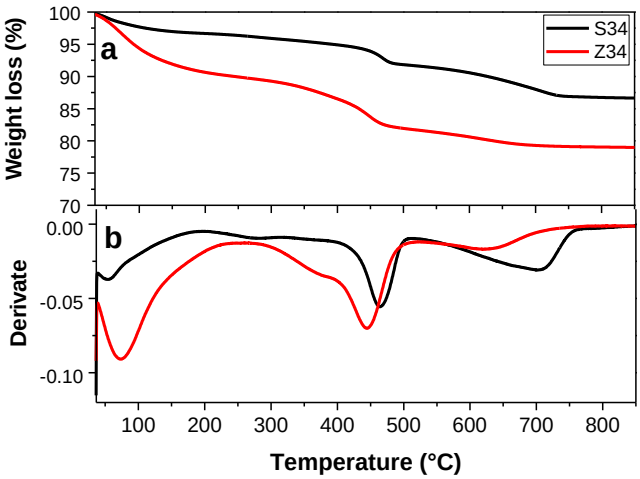

Fig. 4. Thermal analysis of the MeAPSO uncalcined selected materials: TGA **a)** and DTG **b)** of S34 and Z34.

On the other hand, in the curves TGA and DTG, of Z34 and S34 material after calcining (figure not presented), in both cases, a single loss of mass below 100 °C is observed, which corresponds to the physisorption of water retained in the samples. No other significant weight losses are observed a higher temperature which indicates that the SDA was eliminated. For Z34 sample, the isomorphous replacement of P^{5+} by Si^{4+} or Al^{3+} by bivalent metal ions Me^{2+} (as Zn^{2+}) on AlPO framework generates negatively charged framework. In this sample, a negative charge of the framework will be balanced by protonated template. After the removal of the template with calcination, protons will be left attached to the framework oxygen for charge compensation, so in this way, Brönsted acid sites are formed simultaneously. [15, 34]

ICP-OES chemical composition activity

The chemical composition of the molecular sieves is presented in Table 1. The content of Al, P, Si and Zn was determined, and the effective incorporation of zinc was verified in Z34 material. It is known that the (Si + P)/Al ratio should be close to 1 when Si is incorporated into the AlPO structure by the Si directly participating in the crystallization or by the SM2 substitution mechanism with the formation of Si(4Al) species. [35]

Temperature-programmed desorption (NH_3-TPD)

TPD profiles of ammonia desorption from prepared samples are presented in Fig. 5. It can be observed that all samples show a maximum at around 270 °C, indicating that these acid sites are relatively weak, characteristic of this type of materials. The signal is attributed to the hydroxyl groups (–OH) bounded for the defect sites, i.e. POH, SiOH, and AlOH hydroxyl groups [31,15], which were responsible to the weak acidity

J. Mex. Chem. Soc. **2021**, *65*(1)
Special Issue

ISSN-e 2594-0317

of the materials. The specific peak area is proportional to the number of acid sites in the sample and can be determined by integration by convolution of the area under the curve of the spectra. The amounts of weak acid sites of the samples are listed in Table 2.

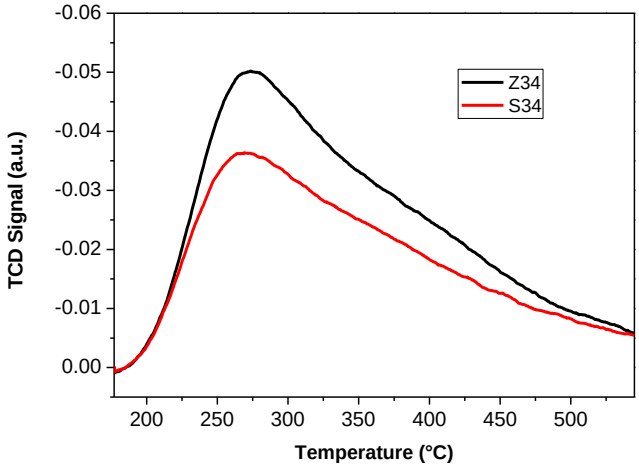

Fig. 5. NH_3-TPD profiles of samples S34 and Z34.

Table. 2. Acid properties of the synthesized materials.

Catalyst	Temperature of maximum (°C)	Acidity (μmol $NH_3 \cdot g^{-1}$)
S34	270	585
Z34	273	859

The Z34 sample shows a higher density of acid sites than the S34 catalyst. It indicates that Zn and Si containing catalyst exhibits much more acid sites compared to S34. Silicon replacement with phosphorous and Zn for aluminum is responsible for of the formation the acid sites in the MeAPSO structures [36]. These results demonstrated that the incorporation of metal ions could adjust the acid intensity and the number of weak acid sites. Calegario et al., [37] mentioned that the incorporation of the metal on SAPO-34 framework in substitution of aluminum atoms, forming acid sites. Thus, the total acid sites concentration increased in a proportion much higher than the amount of metal incorporated. This probably indicates that the metal was helping to disperse the silicon atoms in the crystalline lattice, generating Brönsted acid site. The generation of protonic acidity of SAPO-34 may be explained by the isomorphous substitution mechanisms (SM) of Si in a theoretical framework of $AlPO_4$. The theoretically possible mechanisms are Si for Al (SM1), Si for P (SM2), two Si atoms for one Al and one P, simultaneously, (SM3) in SAPOs. [38]

Catalytic evaluation

The methanol conversion of the SAPO-34 and MeAPSO-34 catalysts in the MTO reaction was investigated at 400 °C with methanol WHSV of 2.12 h^{-1} under atmospheric pressure. The external surface, crystal size and acidity strongly influenced the activity, selectivity and lifetime of the different catalysts. In general, SAPO-34 with CHA cage structure causes a diffusion restriction for olefins, and therefore internal coke formation is the main reason for deactivation [16]. The results shown in Fig. 6 illustrate that, Z34 (MeAPSO-34) exhibited higher catalytic activity with full methanol conversion at short reaction time and longer catalytic life compared to the S34. This can be attributed to two different factors: first, the smaller crystal size which allows the rapid diffusion of the products to the reaction media, avoiding subsequent transformations of the

J. Mex. Chem. Soc. **2021**, *65*(1)
Special Issue

ISSN-e 2594-0317

olefins to heavier products which deactivate the catalyst; second, the presence of stronger acid centers in this sample confirmed by TPD-NH_3 due the incorporation of Zn^{2+} ions [6].

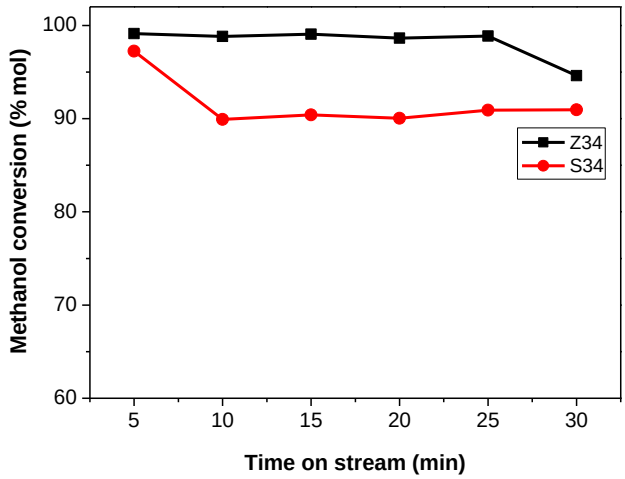

Reaction conditions: WHSV= 2.12 h^{-1}, 400 °C, 1 g of catalyst.

Fig. 6. Methanol conversion in MTO reaction over S34 and Z34 catalysts.

The product selectivity to olefins versus time-on-stream (TOS) over two samples are shown in Fig. 7, for both catalysts, light olefins, are the main products (70−80 % in total), indicating that even in different sizes, all the synthesized SAPO-34 catalysts are very selective for the production of light alkenes from methanol. However, the modified Z34 catalyst had a big impact on the proportion among the selectivity to light olefins (ethylene, propylene, and butylene). As it is shown in Fig. 7, olefins production over S34 and Z34 catalysts increased with an increase in the reaction time. The light olefins selectivity was initially 78 % and 74 % for Z34 and S34 catalysts, respectively. After 30 min of reaction the selectivity increased to 84 % and 82 % for Z34 and S34, respectively. For the large particles in SAPO-34 material, successive polymerization easily occurs because of the long diffusion length, and the catalyst will deactivate rapidly compared to Z34 material [39].

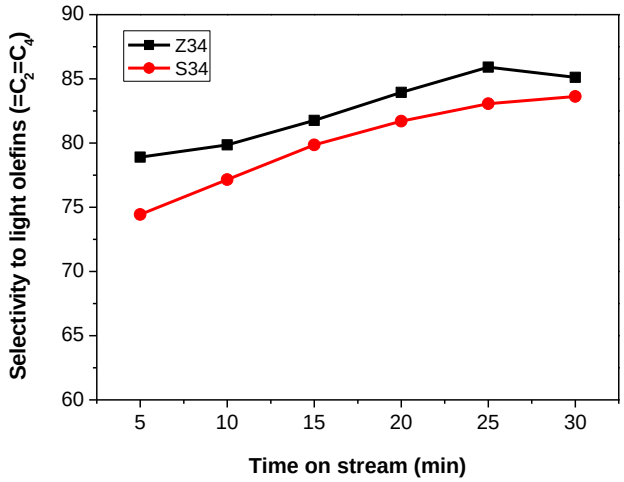

Reaction conditions: WHSV= 2.12 h^{-1}, 400 °C, 1 g of catalyst.

Fig. 7. Selectivity to light olefins ($C_2^=$ - $C_4^=$) over S34 and Z34 catalysts.

J. Mex. Chem. Soc. **2021**, *65*(1)
Special Issue

ISSN-e 2594-0317

The previous study also confirms that the presence of Zn on SAPO-34 material by isomorphic substitution or ionic exchange improved the formation of olefins due of presence of the higher amount of weak sites acid [40,41]. It is concluded that the intrinsic physicochemical properties of zeotypes are greatly affected by Zn and Si incorporation, and remarkably influence their catalytic performances in MTO reaction. Both the Zn as Si content and its location in the zeolites could be very important for the transformation of methanol.

It is well known that SAPO-34 zeotype is widely used in MTO reactions. Therefore, catalytic tests of MTO reaction over SAPO-34 samples have been investigated in a fixed bed reactor at 400 °C [42,43]. Selectivity towards ethylene and propylene over S34 were approximately 28 and 31 % respectively at 5 min on reaction (Fig. 8), and Z34 sample presented a higher selectivity of these olefins (45 y 47 %). Z34 material presented a 0.95 ethylene to propylene ratio, a little higher than that obtained with S34 catalyst, 0.9 ratios. The significant difference in lifetime and selectivity of samples S34 and Z34 catalysts can be explained because MTO is a highly acid-dominating, shape selectivity reaction and crystal size [44]. The reduction of crystal size leads to substantial changes in the properties of the materials, which have an impact on the performance of zeotypes. Smaller material crystals have reduced diffusion path lengths due to the present a longer external surface areas and high surface activity [45].

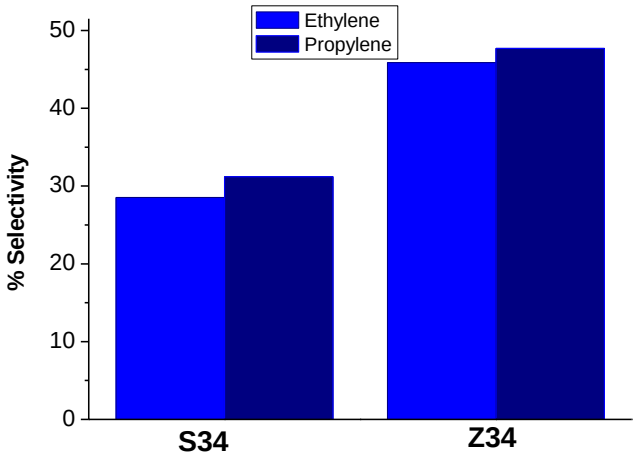

Reaction conditions: WHSV= 2.12 h^{-1}, 400 °C, 1 g of catalyst, reaction time= 5 min.

Fig. 8. Selectivity to ethylene and propylene over S34 and Z34 catalysts.

In our previous works [46] we reported results on the MTH reaction (Methanol-To-Hydrocarbons) of the Zn- modified MeAPSO-36 material (denoted as Z36). This catalyst was active for obtaining aromatics due to its structure formed by larger channels (7.4 x 6.5 Å) and ATS structure that gives rise to the formation of larger molecules and that Zn performance as an aromatizing agent. Fig. 9 shows a comparison in the selectivity to light olefins at 400 °C between material Z34 (from this work) and material Z36 doubly modified with zinc and silicon. The difference between the two catalysts is notable due to their different topologies, sites acid density (151.6 µmolNH_3/g) and average particle (18 µm for Z36). The high activity of MeAPO-36 materials (Me^{2+}, Al and P) for obtaining aromatics has been previously studied by some authors [47]. Selectivity to total aromatics is related to the amount of Zn incorporated into the MeAPSO-36 structure and to the average particle size, a higher molar concentration of Zn, greater selectivity to aromatics compounds.

J. Mex. Chem. Soc. **2021**, *65*(1)
Special Issue

ISSN-e 2594-0317

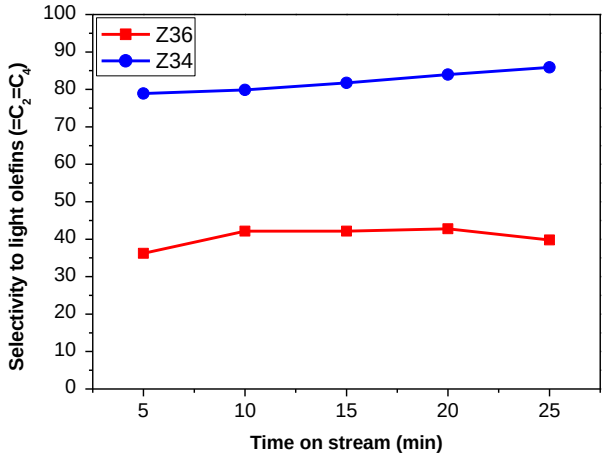

Reaction conditions: WHSV= 2.12 h^{-1}, 400 °C, 1 g of catalyst.
Fig. 9. Selectivity to light olefins ($C_2^=$ - $C_4^=$) over Z36 and Z34 materials.

Conclusion

SAPO-34 zeotype and modified-Zn SAPO-34 were prepared using TEA as SDA and used as catalysts for MTO reaction. The results show that the incorporation of Zn^{2+} promising modification had great effects on crystal size and acidity of the molecular sieves and thus determines their catalytic performance in MTO reaction. The combination of the high external surface and small crystal size, facilitating the accessibility of the reactant molecules to the acid sites, together with the stronger acidity of sample Z34 could be the reasons to explain the better catalytic performance of this catalyst prepared. This catalyst exhibited excellent catalytic performance in MTO reaction with ca. 100 wt% of methanol conversion, ca. 78 % of selectivity to light olefins and ca. 0.95 of ethylene to propylene ratio. Finally, the Z34 catalyst was highly selective for the formation of light olefins compared to the Z36 material (MeAPSO-36) due to topological differences, acid site density, and average particle sizes.

Acknowledgements

The authors thank the Spanish Research Agency -AEI- and the European Regional Development Fund -FEDER- for the funding of this work, through the Projects MAT2016-77496-R (AEI / FEDER, EU) and PID2019-107968RB-I00 (AEI). MGR thanks the Molecular Sieves Group of the Institute of Catalysis and Petrochemistry (CSIC) in Madrid and CONACyT for the support granted for the research stay in Spain.

References

1. Dai, W.; Wang, X.; Wu, G.; Guan, N.; Hunger. M.; Li L. *ACS Catal.* **2011**, *1*, 292–299.
2. Yahyazadeh-Saravi, S; Taghizadeh, M. *Ind. Eng. Chem. Res*. **2019**, *42*, 1640–1662.
3. Hashemi, F.; Taghizadeh, M.; Darzinezhad-Rami, M.; *Micropor. Mesopor. Mater.* **2020**, *295*, 109970
4. Stocker, M.; *Micropor. Mesopor. Mater.* **1999**, *29*, 3–48.
5. Tian, P.; Wei, Y.; Ye, M.; Liu, Z. *ACS Catal*. **2015**, *5*, 1922-1938.

J. Mex. Chem. Soc. **2021**, *65*(1)
Special Issue

ISSN-e 2594-0317

6. Álvaro-Muñoz, T.; Márquez-Álvarez, C.; Sastre, E. *Catal. Today* **2012**, *179*, 27-34.
7. Zhu, J.; Cui, Y.; Nawaz, Z.; Wang, Y.; Wei, F. *Chin. J. Chem. Eng*. **2010**, *18*, 979–987.
8. Dai, W.; Wu, G.; Li, L.; Guan, N.; Hunger, M. *ACS Catal*. **2013**, 3, 4, 588–596.
9. Wilson, S.T.; Lok, B.M.; Messina, C.A.; Cannan, T.R.; Flanigen E.M. *JACS* **1982**, *104*, 1146-1147.
10. Makarova, M.; Ojo, A.; Al-Ghefaili, K.; Dwyer, J. In: Proceedings of the IX International Zeolite Conference. Montreal, Canada **1992**, *2*, 259.
11. Kumar-Saha, S.; Waghmode, S.B.; Maekawa, H.; Kawase, R.; Komura, K.; Kubota, Y.; Sugi, Y. *Micropor. Mesopor. Mater*. **2005**, *81*, 277–287.
12. Wilson, S.T.; Barger, P. *Micropor. Mesopor. Mater*. **1999**, *29*, 117–126.
13. Sławiński, W.A.; Wragg, D.S.; Akporiaye, D.; Fjellvåg, H. *Micropor. Mesopor. Mater*. **2014**, *195*, 311-318.
14. Luo, M.; Zang, H.; Hu, B.; Wang, B.; Mao, G. *RSC Advances* **2016**, *6*, 17651- 17658.
15. Dubois D.R.; Obrzut D.L.; Liu J.; Thundimadathil J.; Adekkanattu P. M.; Guin J.A.; Punnoose A.; Seehra M.S. *Fuel Process. Technol*. **2003**, *83*, 203–218
16. Kang, M. *J. Mol. Catal. A Chem*. **2000**, *160*, 437–444.
17. Ristic, A.; Novak Tusar, N.; Arcon, I.; Thibault-Starzyic, F.; Hanzel, D.; Czyzniewska, J.; Kaucic, V. *Micropor. Mesopor. Mater*. **2002**, *56*, 303-315.
18. Salmasi, M.; Fatemi, S.; Najafabadi A.T. *J. Ind. Eng. Chem.* **2011**, *17*, 755–761.
19. Sun, C.; Wang, Y.; Wang, Z.; Chen, H.; Wang, X.; Li, H.; Sun, L.; Fan, C.; Wang, C.; Zhang, X. *Compt. Rendus Chim*. **2018**, *21*, 61–70.
20. Huang, H.; Mengyun, Y.; Zhang, Q.; Li C. *Catal. Commun* **2020**, *137*, 105932.
21. Van Niekerk, M. J.; Fletcher, J. C. Q.; O Connor, C. T. *Appl. Catal. A Gen*. **1996**, *138*, 135–145.
22. Xu, L.; Liu, Z.M.; Du, A.P.; Wei, Y.X.; Sun, Z.G. *Stud. Surf. Sci. Catal*. **2004**, *147*, 445.
23. Sun, Q.; Xie, Z.; Yu, J. *Natl. Sci. Rev*. **2017**, *0*, 1–17.
24. Terasaka, K.; Imai, H.; Li, X. *J. Adv. Chem. Eng.* **2015**, *5*:4, 1000138.
25. Aghaei, E.; Haghighi, M.; Pazhohniya, Z.; Aghamohammadi, S, *Micropor. Mesopor. Mater*. **2016**, *226*, 331-343.
26. Benvindo, F.S.; de Sousa, R.C.; Fernandes, L.D. in: Anais do XX Simpósio IberoAmericano de Catálise, **2006**, volume CDROM, 1–6.
27. Thommes, M.; Kaneko, K, Neimark, A, Olivier, J.P.; Rodriguez-Reinoso, F.; Rouquerol, J.; Sing, K. *Pure Appl. Chem.* **2015**, *87*, 1051–1069.
28. Wang, Q.; Chen, G.; Xu, S. *Micropor. Mesopor. Mater*. **2009**, *119*, 315–321.
29. Basina, G.; Shamia, D.A.; Polychronopoulou, K.; Tzitzios, V.; Balasubramanian, V.V.; Dawaymeh, F.; Karanikolosa, G.N.; Wahedi, Y.A. *Surf. Coat. Tech*. **2018**, *353*, 1-29.
30. Mirza, K.; Ghadiri, M.; Haghighi, M.; Afghan, A. *Micropor. Mesopor. Mater*. **2018**, *260*, 155–165.
31. Izadbakhsh, A.; Farhadi, F.; Khorasheh, F.; Sahebdelfar, S.; Asadi, M.; Zi-Feng, Y. *Appl. Catal. A: Gen.* **2009**, *364*, 48–56.
32. Zhu, Q.; Kondo, N.J.; Ohnuma, R.; Kubota, Y.; Yamaguchi, M.; Tatsumi, T. *Micropor. Mesopor. Mater*. **2008**, *112*, 153–161.
33. Álvaro-Muñoz, T.; Márquez-Álvarez, C.; Sastre, E. *Catal. Today* **2012**, *179*, 27-34.
34. Wei, Y.; Zhang, D.; Xu, L.; Chang, F.; He, Y.; Meng, S.; Su, B.; Liu, Z. *Catal. Today* **2008**, *131*, 262–269.
35. Xu, L.; Du, A.; Wei, Y.; Wang, Y.; Yu, Z.; He, Y.; Zhang, X.; Liu, Z. *Microporor. Mesopor. Mater.* **2008**, *115*, 332.
36. Izadbakhsh, A.; Farhadi, F.; Khorasheh, F.; Sahebdelfar, S.; Asadi, M.; Yan, Z.F. *Micropor. Mesopor. Mater*. **2009**, *126*, 1–7.
37. Calegario-Sena, F.; Figueirôa-de Souza, B.; Caroline-de Almeida, N.; Simonace-Cardoso, J.; Domiciano-Fernandes, L. *Appl. Catal. A: Gen.* **2011**, *406*, 59– 62.
38. Varzaneh, A.Z.; Towfighi, J.; Sahebdelfar, S. *Micropor Mesopor Mater.* **2016**, *236*, 1.
39. Sharifi-Pajaie, H.; Taghizadeh, M. *J. Ind. Eng. Chem*. **2015**, *24*, 59-70.
40. Huang, H.; Yu, M.; Zhang, Q.; Li, C. *Micropor. Mesopor. Mater*. **2020**, *295*, 109971.
41. Zhong, J.; Han, J.; Wei, Y.; Xu, S.; Sun, T.; Guo, X.; Song, C.; Liu, Z. *J. Energy Chem*. **2019**, *32*, 174-181.

J. Mex. Chem. Soc. **2021**, *65*(1)
Special Issue

ISSN-e 2594-0317

42. Sun, Q.; Wang, N.; Bai, R.; Chen, G.; Shi, Z.; Zou, Y.; Yu, J. *Chem Sus Chem*. **2018**, *11*, 3812–3820.
43. Song, W.; Haw, J.; Nicholas, J.; Heeneghan, C. *J. Am. Chem. Soc*. **2000**, *122*, 10726–10727.
44. Pajaie, H.S.; Taghizadeh, M. *J. Ind. Eng. Chem.* **2015**, *24*, 59–70.
45. Tosheva L.; Valtchev V.P. *Chem. Mater.* **2005**, *17*, 2494-2513.
46. García Ruiz, M.; Solís-Casados, D.A.; Aguilar-Pliego J.; Márquez-Álvarez, C.; Sastre de Andrés, E.; Sanjurjo-Tártalo, D.; Sánchez-Sánchez, M.; Grande-Casas M. *Top Catal.* **2020**. DOI: https://doi.org/10.1007/s11244-020-01266-3
47. Akolekar, D.B.; Bhargava, S. *J. Mol. Catal A.* **2020**, *122*, 81–90.